



Catalytic investigation of Pd(II) complexes over Heck–Mizoroki reaction: Tailored synthesis, characterization and density functional theory

SATYENDRA N. SHUKLA^{1*}, PRATIKSHA GAUR¹, SANJAY S. BAGRI¹,
RIPUL MEHROTRA² and BHASKAR CHAURASIA¹

¹*Coordination Chemistry Research Lab, Department of Chemistry, Government Science College, Jabalpur (M.P.) 482001, India* and ²*Instituto de Química Rosario Área Inorgánica Facultad de Cs. Bioquímicas y Farmacéuticas Universidad Nacional de Rosario Suipacha 531 S2002LRK Rosario, Argentina*

(Received 2 September, revised 18 November, accepted 20 November 2020)

Abstract: Tailored reaction of Schiff base ligands with palladium(II) chloride and imidazole afford three complexes of formula $[Pd^{(II)}(L)(imdz)_2]Cl$, which are L = 2-((E)-(p-lylimino)methyl)-6-methoxyphenol (complex **1**), 2-methoxy-6-((E)-(phenylimine)methyl)phenol (complex **2**) and 2-((E)-(4-chlorophenylimino)methyl)-6-methoxyphenol (complex **3**). Compounds were characterized with elemental analysis, molar conductance, electronic spectroscopy, ESI-MS, FT-IR, TGA, ¹H-NMR and ¹³C-NMR. Molecular structure and different quantum chemical parameters were calculated using the B3LYP basis set of density functional theory with the standard 6-311+G (d, 2p) level. The catalytic potential of **1–3** was examined over Heck-Mizoroki reaction and found in order of **1 > 2 > 3**.

Keywords: Schiff base Pd(II) derivative; spectroscopic characterization; molecular modeling; thermogravimetric analysis; cross-coupling reaction.

INTRODUCTION

The cross-coupling reactions leading to C–C bond formation have emerged recently as a remarkably significant preparative strategy for the synthesis of various class of organic compounds.¹ The catalytic introduction of C–C bond to any organic moiety is one of the most popular methods for the synthesis of large complex organic molecules.² These methods have been successfully employed in the synthesis of many natural products, bioactive compounds and materials. Despite the presence of several other C–C bond formation reactions, like Suzuki, Sonogashira, Tsuji-Trost, Negishi and Hiyama-coupling reactions, Heck–Mizoroki reaction has attained significant position during the last ten years due to vari-

* Corresponding author. E-mail: ccrl_2004@rediffmail.com; sns1963_1@rediffmail.com
<https://doi.org/10.2298/JSC200902075S>

ous applications, *viz.* pharmaceuticals, agrochemicals, synthetic fragrances, cosmetics, detergents, and other commercial derivatives.^{3–6}

The palladium-catalyzed Heck–Mizoroki cross-coupling reaction has drawn much attention due to high efficiency, chemoselectivity and mild reaction conditions.⁷ The remarkable ability of palladium complexes to assemble C–C bonds between suitable functionalized substrates remain a growing area of research.⁸ The well-accepted mechanism for this reaction (Fig. 1) is based on the intermediate species involving Pd(0)/Pd(II); however, other possibilities cannot be ruled out.⁹ Schiff base metal-derivatives have displayed a wide range of applications, *i.e.*, pharmaceutical, industrial and catalysis.¹⁰ Anchoring of a Schiff base complex by a suitable ligand may be used as a strategy to tune the catalytic activity of complexes.¹¹ Since, imidazole is an electron-rich heterocyclic nucleus with a wide range of applications in medicinal chemistry, non-linear optics and as a catalyst in industrial uses, it was selected as an anchoring ligand.¹²

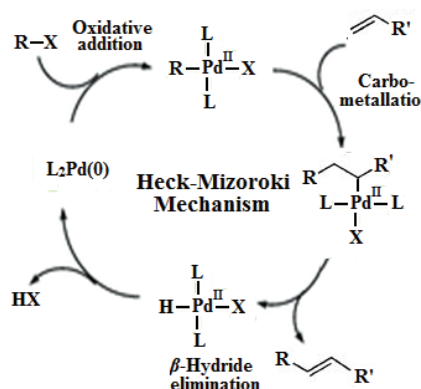


Fig. 1. General mechanism of Heck–Mizoroki reaction.

The present study is an attempt to synthesize an efficient catalyst and investigate the role of palladium intermediates formed in the Heck–Mizoroki mechanism.¹³ Although some studies have been done in the field, a lot still remains to be investigated.¹⁴ Therefore, we have synthesized Schiff base ligands through condensation of 4-hydroxy-3-methoxy-benzaldehyde popularly known as *o*-vanillin with selected amines. The resulting ligands in combination with imidazole as a complementary ligand yielded the novel three Pd(II) derivatives. Thus, we herein, report new palladium(II) Schiff base complex as an efficient catalyst in Heck–Mizoroki cross-coupling reaction. Density functional theory (DFT) is a computational quantum mechanical modelling method used to investigate the electronic structure of many-body systems, in a particular molecules. DFT was used to optimize the geometry of synthesized compounds in the gaseous phase. The probable mechanism of the catalysis and energy profile diagram was also elucidated. A general scheme for the synthesis of ligands and complexes is given in Fig. 2.

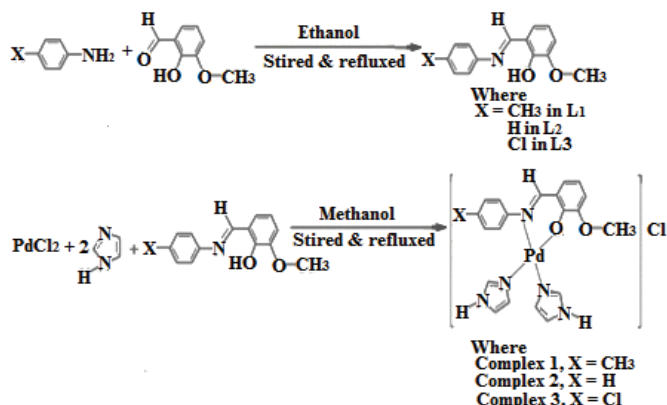


Fig. 2. Scheme for the synthesis of ligands and complexes

EXPERIMENTAL

Materials and methods

Palladium(II) chloride and other starting materials were purchased from E. Merck, India/Sigma Aldrich and used as received. Analytical reagent grade solvents were used. Conductivity measurements were carried out at 25 °C on an EI-181 conductivity bridge with dipping type cell. ESI-MS spectra were recorded on Agilent-6520(QTOF) mass spectrometer. FT-IR spectra were recorded in KBr pellets on Shimadzu-8400 PC. Electronic absorption spectra were recorded with EI-2305, double beam spectrophotometer equipped with a PC. ¹H-NMR and ¹³C-NMR spectra were recorded in DMSO-*d*₆ on Agilent-700-vnmrs 700. The metal contents were analyzed gravimetrically by the literature procedure.¹⁵ For the catalytic investigation, degassed solvents were used with bubbling nitrogen for 50 min.

Synthesis of Schiff base ligands 2-((E)-(p-tolylimino)methyl)-6-methoxyphenol (L₁)/2-methoxy-6-((E)-(phenylimino)methyl)phenol (L₂)/2-((E)-(4-chlorophenylimino)methyl)-6-methoxyphenol (L₃)

Ligands were prepared according to the method reported in the literature.^{16–18} The solids obtained in each case were filtered off, washed several times with ethanol and recrystallized with hot methanol to yield orange/yellow crystals which were dried over anhydrous calcium chloride in desiccators under vacuum.

Synthesis of complexes[Pd(L)(imdz)₂]Cl; where L = Schiff base ligand L₁/L₂/L₃

Palladium(II) chloride (0.177 g, 0.001 mol) and imidazole (0.136 g, 0.002 mol) were mixed in 25 mL methanol and stirred at room temperature for 30 min to 1 h. Schiff base ligand, **SB** (0.001 mol) dissolved in 25 mL hot methanol was added to the above reaction mixture. The resulting reaction mixture was stirred for 2–3 h in an inert atmosphere. A brown/light brown/dark brown solid was separated after refluxing the reaction mixture for 6–8 h, which was filtered, washed with diethyl ether, and dried in vacuum. Unfortunately, after several attempts, we did not find any crystal suitable for single-crystal XRD.

DFT calculation

Density functional theory (DFT) was employed to achieve more insight into the molecular structure. It was carried out using the method of B3LYP with 6-311++G(d,p) basis set

for all nonmetallic atoms and Los Alamos National Laboratory 2 double zeta (LANL2DZ) basic set for the central metal atoms in the gas phase.¹⁹ Gaussian-09 software package was employed to carry out all the quantum chemical calculations.²⁰ Optimized structural parameter of the compounds such as bond lengths, bond angles and dihedral angles were calculated with the atom numbering scheme of the molecule. Several quantum chemical parameters have been calculated.²¹ The ¹H-NMR and ¹³C-NMR Chemical Shifts of the molecule were calculated by the gauge-independent atomic orbital (GIAO) method and compared with the experimental results. DFT was employed to study the energy profiles of the full catalytic cycle of complex **1** for the Heck-Mizoroki reaction.

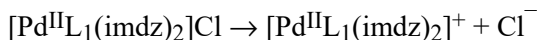
Catalytic activity over Heck–Mizoroki reaction

The solvent mixture (DMF:H₂O in 1:1 ratio) used in reaction was degassed through the Freeze-pump-claw method.²² A three-neck round bottom flask equipped with water condenser, magnetic stir bar and N₂-inlet was charged with degassed DMF: H₂O (100 mL), potassium carbonate (0.75 mmol) and complex (**1–3**, 0.4 μmol). The styrene (0.6 mmol) and aryl halide (0.5 mmol) were added by glass syringe through a rubber septum. The mixture was allowed to stir at ~80 °C for 8 h and then cooled to room temperature. It was further filtered through the bed of silica. The reaction progress was monitored periodically by TLC. The product was extracted with ethyl acetate (3×10 mL). The combined organic phase was washed with brine (2×10 mL) and dried over Na₂SO₄. The solvent was removed under reduced pressure to afford impure residue. The residue obtained was purified through column chromatography on silica gel eluting with ethyl acetate. Column chromatography was performed to obtain a purified product. The pure compound was obtained by eluting the column by ethyl acetate:hexane (5:95 volume ratio) solvent mixture.

RESULTS AND DISCUSSION

Spectral characterization of complexes

Stoichiometries of the complexes were in agreement with elemental analyses data. Molar conductance (Λ_m) for complexes in 10⁻³ M concentration in DMSO was in the range 16–19 Ω⁻¹ cm² mol⁻¹ indicative of their 1:1 electrolytic nature.²³ ESI-MS spectra of complexes exhibit several peaks. However, a pseudo-molecular ion peak for [M+H⁺] was inevitably present in each case, which indicates the molecular mass. ESI-MS spectrum of complex **1** is shown in Supplementary material to this paper, Fig. S-1. This shows a signal for [M⁺], confirming 1:1 electrolytic nature of complex **1**, probably due to dissociation in solution as below:



In the FT-IR spectra of complexes, the band observed at ~3217 cm⁻¹, assigned for –OH vibration in ligands completely vanished and a new band at lower frequency appeared at ~534 cm⁻¹, which was assigned to Pd–O.²⁴ The appearance of this band indicates the bonding of metal with phenolic oxygen. The band due to azomethine HC=N groups was shifted downwards in complexes and observed at ~1602 cm⁻¹, which confirms the coordination of azomethine nitrogen with metal. The coordination of azomethine nitrogen with metal was

further ascertained by the appearance of a band at a lower frequency at $\sim 450\text{ cm}^{-1}$, assign to Pd–N vibration stretching.²⁵ The experimental FT-IR spectrum of complex **1** was compared with the theoretical I.R. spectrum and presented in Table S-I (Supplementary material). Since the DFT calculation generally overestimates the vibrational frequencies due to the neglect of crystal packing effects and anharmonicity, as well as incompleteness of the basis set and dynamic electronic correlation, the calculated frequencies slightly deviated from the experimental values of the normal vibrations. Therefore, we have derived scaling factors and applied to the theoretical data to get a satisfactory value. On comparison, it was observed that the in the theoretical spectra after scaling peak for $\nu(\text{C}-\text{H})$, $\nu(\text{HC}=\text{N})$, $\nu(\text{C}-\text{O})_{\text{sym}}$, $\nu(\text{C}-\text{O})_{\text{asym}}$, $\nu(\text{C}-\text{H}_3)_{\text{in plane}}$, $\nu(\text{C}-\text{H}_3)_{\text{out plane}}$, $\nu(\text{Pd}-\text{O})$ and $\nu(\text{Pd}-\text{N})$ were observed with a deviation of 0.1 %. The calculated scaling factor for complex **1** is 1.000 ($R^2 = 0.999$) over a complete range of the spectrum. From Table S-I, it can be observed that most of the unscaled vibrations become closer to the experimental value after scaling. The experimental and theoretical FT-IR spectrum of complex **1** is shown in Fig. S-2 of the Supplementary material.

Complexes are diamagnetic as expected for d^8 configuration.²⁶ In electronic spectra, the lowest energy band at $\sim 703\text{ nm}$ was assigned to ${}^1\text{A}_{1g} \rightarrow {}^3\text{A}_{2g}$ (v_1) transition. However, bands at ~ 605 , ~ 440 and $\sim 400\text{ nm}$ were attributed to ${}^1\text{A}_{1g} \rightarrow {}^1\text{A}_{2g}$ (v_2), ${}^1\text{A}_{1g} \rightarrow {}^1\text{E}_g$ (v_3) and ${}^1\text{A}_{1g} \rightarrow {}^1\text{B}_{1g}$ (v_4) transitions, indicating square-planar geometry around Pd(II) ion.²⁷ The spectrum of complex **1** is given in Fig. S-3 of the Supplementary material.

The coordination of the azomethine HC=N group was confirmed by the downfield shifting of the azomethine proton signal in complexes by δ 0.08–0.09 ppm. This downfield shifting of azomethine proton in Pd(II) complex was attributed to the discharge of the electronic cloud towards the Pd(II) ion. The hydroxyl OH proton signal at $\delta \approx 13.30\text{ ppm}$ in the ligands disappeared in the spectra of Pd(II) complexes, indicating the deprotonation and the coordination of oxygen with the metal ion. The ${}^1\text{H-NMR}$ spectrum of the complexes shows doublet centred at $\delta \approx 10.85\text{ ppm}$ for two protons attributed to the –NH of two imidazole ring. A doublet at $\delta \approx 7.30\text{ ppm}$ for two C–H protons and a multiplet centred at $\delta \approx 7.25\text{ ppm}$ for four protons were assigned to other C–H protons of the imidazole ring.³⁰ The two double doublets centred at $\delta \approx 7.10\text{ ppm}$, $\delta \approx 6.90\text{ ppm}$ ($J \approx 8$ and $\approx 2.5\text{ Hz}$) and a triplet centred at $\delta \approx 6.77\text{ ppm}$ ($J \approx 8.0\text{ Hz}$) were attributed to aromatic protons of vanillin moiety. However, in complex **1** and **3**, a multiplet centred at $\delta \approx 7.20\text{ ppm}$ for four protons was attributed to toluidine/chloroaniline moiety. In complex **2**, a multiplet centred at $\delta \approx 7.22\text{ ppm}$ for five protons was assigned for aniline moiety. In addition to this, in complexes, a signal at $\delta \approx 3.45\text{ ppm}$ was assigned for protons of methoxy group. In complex **1**, a signal at $\delta = 2.22\text{ ppm}$ was assigned for methyl proton. The theoretical chemical shift values were calculated by the GIAO method using TMS-HF/6-31G(d)

GIAO and TMS-B3LYP/6-311+G(2d, p) GIAO level theory. The correlation coefficients of ^1H -NMR were determined as 0.979 and 0.985 as given in Fig. S-4A and B of the Supplementary material. For L_1 , ^1H -NMR $\delta_{\text{cal}} = 1.135\delta_{\text{exp}} - 1.193$ ($R^2 = 0.979$). For complex **1**, ^1H -NMR $\delta_{\text{cal}} = 0.987\delta_{\text{exp}} - 0.196$ ($R^2 = 0.985$). It was evident from the correlation graph that a good correlation exists in theoretical and experimental δ values. ^1H -NMR of the spectrum of complex **1** is shown in Fig. S-5 of the Supplementary material.

In ^{13}C -NMR spectrum signal at $\delta \approx 160.0$ ppm in ligand assigned for azomethine group was downfield shifted by $\delta = 3.4 - 6.2$ ppm in the complexes confirming the transfer of one lone pair electron from nitrogen to metal and coordination of azomethine-N to metal. In complexes, the two signals appeared at $\delta \approx 135.0$ ppm were assigned for the two imidazole ring carbon atom. The remaining four imidazole carbon resonate at $\delta \approx 120.0$ ppm. In complex **1** and **3**, the six signals observed between $\delta = 156.6 - 130.0$ ppm were attributed to vanillin moiety of the ligand. In complex **2**, the six signals of vanillin carbon appeared between $\delta = 153.1 - 126.6$ ppm. However, the remaining six signals observed between $\delta = 129.0 - 111.1$ ppm were ascribed for six-carbon of toluidine/aniline/*p*-chloroaniline ring moiety. A signal in complexes observed between $\delta = 55.8 - 52.6$ ppm was assigned for methoxy carbon. In complex **1**, a signal at $\delta = 20.5$ ppm was due to methyl carbon of vanillin moiety. The correlation coefficients of ^{13}C -NMR for L_1 and complex **1** were determined as 0.977 and 0.999, as shown in Fig. S-6A and B of the Supplementary material. It was evident from the correlation graph that a good correlation exists in theoretical and experimental δ values. The ^{13}C -NMR spectrum of complex **1** is shown in Fig. S-7 of the Supplementary material.

TGA of complexes (Fig. 3A, B and C) were carried out in the temperature range of 30–900 °C at the heating rate of 10 °C/min in a nitrogen atmosphere. The TGA curves of these complex displayed a similar two steps degradation pattern. In each case, the first step was the partial decomposition of ligand and one imidazole unit along with one Cl^- . In the second step, the loss of the remaining one imidazole unit occurs. In complex **1**, a weight loss of 64 % (calcd. 63.34 wt.%) in the temperature range ~255–350 °C was attributed to the first step of decomposition. In second step the loss of remaining one imidazole unit occurs in the temperature range of 350–530 °C, with a weight loss of 13 % (calcd. 12.45 wt.%). In complex **2**, a weight loss of 62.52 % (calcd. 62.22 wt.%) in the temperature range ~330–370 °C was attributed for the first step decomposition. In the second step the loss of remaining one imidazole unit occurs in the temperature range of 370–500 °C with a weight loss of 13.46 % (calcd. 13.51 wt.%). In complex **3**, a weight loss of 64.93 % (calcd. 64.64 wt.%) in the temperature range ~330–390 °C was the first step of decomposition. In the second step loss of remaining one imidazole unit occurs in the temperature range of 390–500 °C, with a

weight loss of 12.38 % (calcd. 12.61 wt.%). A very unusual gain of weight in complex **1** between 500–600 °C is ascribed to the oxidation of the remaining Pd to PdO. In the end, a metallic oxide residue was formed as PdO (calcd. 22.45 wt.%).^{28–30}

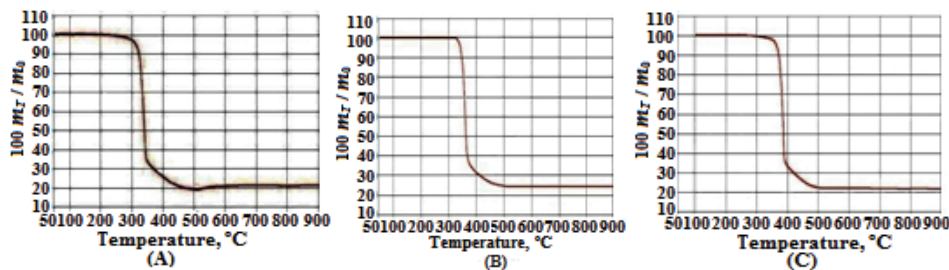


Fig. 3. TGA curve of complexes: A) **1**, B) **2** and C) complex **3**.

Quantum chemical calculations

Mulliken atomic charge and molecular electrostatic potential analysis (MEP).

The calculated Mulliken atomic charge values of selected atoms were listed in Table S-II of the Supplementary material. Mulliken atomic charge plots of rest of the ligands and complexes were given in Fig. S-8 of the Supplementary material. From results, it was observed that in ligands the hydrogen attached with the electronegative oxygen exhibits the highest positive charge of ~ +0.4000. However, the highest negative charge of ~ -0.6800 was present on highly shielded oxygen. However, in complexes **1–3**, the highest positive charge of ~ +0.4700 was present at Pd metal centre. The other electronegative atoms such as phenolic oxygen and azomethine nitrogen consist of a negative Mulliken charge because of high electron density on these atoms. The imidazole ring is an electron-rich moiety, and its N atoms possess the negative Mulliken charge. The Mulliken charge values of electropositive carbon and electronegative oxygen/nitrogen are also higher than ligand, probably due to the occurrence of back bonding of π -electrons during complexation. This result is consistent with the molecular electrostatic potential map.³¹ The molecular electrostatic potential (MEP) is a particularly useful descriptor in understanding sites for electrophilic and nucleophilic reactions as well as hydrogen-bonding interactions. The molecular electrostatic potential, (r), at a given point r (x , y , z) in the vicinity of a molecule is defined in terms of the interaction energy between the electrical charge generated from the molecule electrons and nuclei. To predict the electrophilic and nucleophilic reactive sites for the title molecule, MEP was calculated using the B3LYP/LanL2DZ method with the 6-31++G(d,p) basis set and optimized geometries. The negative (red) regions of MEP were related to electrophilic reactivity and the positive (blue) regions to nucleophilic reactivity. The MEP maps of ligands and complexes were shown in Fig. S-9 of the Supplementary material. The electrostatic potential in **L**₁

ranges between -5.7×10^{-2} to 5.7×10^{-2} a.u. and in **L**₂ it ranges from -5.6×10^{-2} to 5.6×10^{-2} a.u. Similarly, in **L**₃, potential value is found between -6.1×10^{-2} to 6.1×10^{-2} a.u. The electrostatic potential in complex **1** range between -9.2×10^{-2} to 9.2×10^{-2} a.u. and in complex **2**, it ranges from -9.7×10^{-2} to 9.7×10^{-2} a.u. Similarly, in complex **3**, potential value is found between -9.8×10^{-2} to 9.8×10^{-2} a.u. Different colours represent the different values of the electrostatic potential at the surface. The potential increases in the order: red < orange < yellow < green < blue.³² It was observed that the positive areas are present on less electronegative atom such as hydrogen, carbon, and central metal atoms. On the other hand, the negative areas are confined on more electronegative O, and N. These electronegative moieties worked as a donor atom of the ligand.

Molecular modelling and computational study. The quantum chemical parameters were calculated and listed in Table S-III. The highest occupied molecular orbital (HOMO) and the lowest unoccupied molecular orbital (LUMO) are named as frontier molecular orbitals (FMO). The HOMO and LUMO of **L**₁ and complex **1** is shown in supplementary Fig. S-10 of the Supplementary material. The HOMO and LUMO energies and energy gap, ΔE of ligands and complexes were given above in Table S-III. From the calculated energies of the highest occupied molecular orbital (HOMO) and lowest unoccupied molecular orbital (LUMO), it may be concluded that:

1. The difference of FMOs energies in complexes are for E_{HOMO} is in the order **L**₃ > **L**₂ > **L**₁ > **3** > **1** > **2** and for E_{LUMO} the order is **3** > **2** > **1** > **L**₃ > **L**₁ > **L**₂.
2. Complex **2** has low values of the energy gap (ΔE) suggesting high reactivity.
3. Complex **1** exhibit a high value of the dipole moment, which may favour their dipole-dipole interactions between molecules.

Bond length and bond angle. The optimized structures of the complexes with the atomic numbering scheme were determined. The bond lengths (Å) and bond angles (in degree) obtained from the geometry optimized structures are given in Tables S-IV and S-V. The molecular structure of complexes exhibits almost square planar geometry around the metal centre, as revealed from the calculated bond lengths and bond angles. The C=N, C–O and C–C bond lengths become slightly longer in complexes than the bonds formed with ligands. Ligands were coordinated *via* imine nitrogen by the shifting of electron density of imine and phenolic oxygen because of the removal of phenolic hydrogen. Formation of two new bonds Pd–N and Pd–O takes place. The C–O bond distance in all complexes becomes longer due to the formation of Pd–O bond, which makes the C–O bond weaker. This elongation in Pd–N and Pd–O bond lengths caused a slight distortion from the regular square planar geometry.

Thus, based on the elemental analysis, ESI-MS, molar conductance, electronic spectra, FT-IR, ^1H -NMR, ^{13}C -NMR, TGA and DFT studies, the optimized structures of the ligands and complexes are given in Fig. 4A–F.

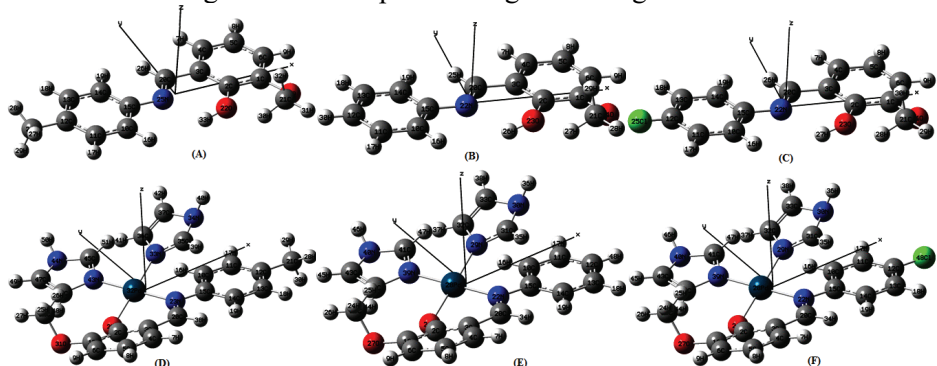


Fig. 4. DFT optimized structure of: A) \mathbf{L}_1 , B) \mathbf{L}_2 , C) \mathbf{L}_3 , and complexes: D) $\mathbf{1}$, E) $\mathbf{2}$ and F) $\mathbf{3}$.

Catalytic activity

Catalytic potential for the synthesized complexes was examined over Heck–Mizoroki C–C cross-coupling reaction (Fig. 5) at various reaction conditions of temperature, base, solvent and catalyst loading. The results obtained are summarized in Table S-VI.

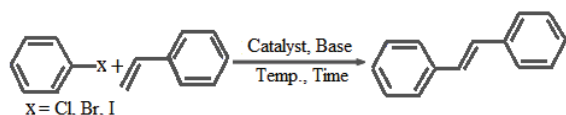


Fig. 5. Scheme for catalytic activity optimization.

Effect of catalyst loading/base/solvent and temperature. It is ideal to have good yields using a minimal amount of catalysts. Hence, this study examined the effect of catalyst loading (0.1–0.6 μmol). It was observed that the highest yield of a coupling product was obtained when 0.4 μmol of the complex **1** was employed as a catalyst. Higher product conversion with an increased amount of catalyst may probably due to the increased availability of more basic sites, which can be linked to the dispersion of more active species.³³ However, with the increasing catalyst concentration above 0.4 μmol , no appreciable increase in product yield was observed. The yield of products at different catalyst concentration is shown in Fig. 6A.

The role of a base is to neutralize the acid and consequently the exchange of a hydrogen atom with an aryl or vinyl group occurs. Hence, to study the effect of the base in Heck–Mizoroki reaction, the reaction was carried out in the presence of different bases such as K_2CO_3 , Na_2CO_3 , CH_3COONa , NaOH and KOH . It

was observed from Fig. 6B that K_2CO_3 is the most effective base in the catalytic conversion, probably due to its higher solubility in comparison to others.

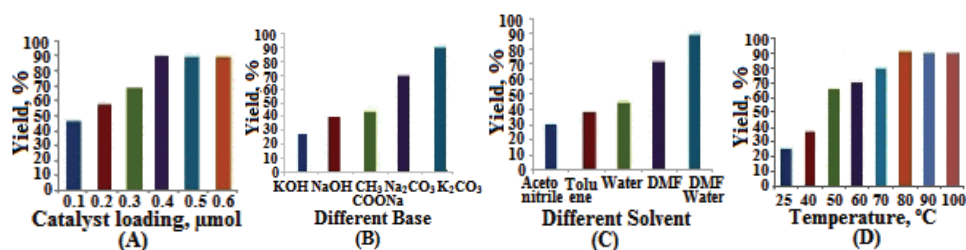


Fig. 6. Heck–Mizoroki reaction; A) effect of catalyst loadings, B) effect of different base, C) effect of different solvents, D) effect of temperature.

It was observed that the mixed solvent such as DMF+ H_2O (1:1) gives good quantitative yield. The polar aprotic solvents such as the DMF give a lower yield. However, in acetonitrile solvent, lowest yield of product was obtained, as shown in Fig. 6C. Heck–Mizoroki reaction is a temperature-sensitive reaction, and therefore it is necessary to study the reaction at different temperature ranges from 25–100 °C. It was observed that, at room temperature, very little catalytic conversion takes place, and with the rise of temperature the yield increases. The maximum yield was observed at an optimum temperature of 80 °C. With further increase of the temperature, no appreciable increase in yield was observed. The temperature effect can be explained by the influence on the equilibrium between different forms of Pd participating in the reaction. For example, the low-temperature decrease provides the increase of the stability of palladium complexes in solution. In contrast, higher temperature increases the rate of Pd reduction. The percentage yield at different reaction temperature is shown in Fig. 6D.

With the optimized reaction conditions in hand, the scope of the Heck–Mizoroki reaction was extended to a variety of substituted aryl halides (XC_6H_4Y ; where X = Br/Cl/I and Y = H/ CHO/OCH₃). It was interesting to observe that the yield of the product is almost the same in the case of bromo and iodobenzene. However, in the case of aryl bromide substituted with electron-withdrawing aldehydes group (Table S-VII, entry 4) higher yield was observed in comparison to a substrate with an electron-donating methoxy group (Table S-VII, entry 5). The reaction of chlorobenzene, in comparison to bromobenzene/iodobenzene, failed in providing good yield under optimized conditions presumably owing to less reactivity of C–Cl bond due to higher bond energy. Turn over frequency (TOF) of catalysts was also calculated, and it ranges between 36.3–302.5 h⁻¹. TOF values are higher than the reported TOF values in similar complexes.³⁴ The catalytic activity of the complex **1** was quite good in comparison to previously reported catalysts for Heck–Mizoroki coupling reaction in terms of temperature, cat-

alyst loading, base and solvents.³⁵ In our case catalyst gave better yields at moderate temperature using less amount of catalyst in the DMF–water medium. ¹H-NMR and ¹³C-NMR characterized the resulting products.

Energy profile diagram. DFT calculations were performed at the B3LYP/6-31G level of theory to evaluate the formation of alkene *via* C–C cross-coupling reaction using chelated palladium Schiff base complex **1** as a catalyst. The overall computed energy profile diagram of this reaction is displayed in Fig. 7. The energy profile diagram shows that the complete Heck–Mizoroki reaction proceeds *via* four major steps, *viz.* reductive elimination, oxidative addition, migratory insertion and β -hydride elimination. The first step involves the elimination followed by the reduction of Pd(II) to Pd(0). Reductive elimination is a facile step with an energy barrier of 2.0116 eV. The next step involves the addition of Ph-Br and oxidation of metal center Pd(0) to Pd(II) with the energy of 2.4116 eV. After that, the formation of high energy π -complex **TS**₁ takes place which later gets stabilized by 1.0386 eV and forms a stable sigma intermediate **TS**₂. Sigma complex further changes into a new higher energy state **TS**₃ by the migratory insertion mechanism. In the last step, β -hydride elimination occurs, and a final cross-coupled product was obtained. The energy profile of reaction obtained from the DFT calculation clearly shows that π -complex **TS**₁ is situated at the top in comparison to **TS**₂ and **TS**₃. The less stable energetically **TS**₃ is more favourable for easy conversion into the product. There has been considerable evidence that oxidative addition does not limit the rate of Heck–Mizoroki reactions.³⁶ Further evidence from the gas-phase computational studies indicates that the rate-determining step in a palladium (II/IV) cycle involving iodobenzene would be the oxidative addition of iodobenzene to palladium. Since the actual rate-determining step in the Heck–Mizoroki reaction of aryl iodides is not oxidative addition, this indicates that palladium (II/IV) cycle is not running. In the present situation, we suggest olefin coordination as a rate-limiting step, due to wide energy gap in between **3** and **4** in the energy profile diagram of the catalytic cycle. The probable mechanism of Heck–Mizoroki reaction is shown in Fig. S-11 of the Supplementary material.

CONCLUSION

Three novel mixed ligand complexes of Pd(II) containing imidazole as anchoring ligand and Schiff base as N, O donor, have been synthesized by the tailored synthesis and characterized. For a better insight into molecular structure, quantum chemical calculations have been performed. The geometry of compounds was optimized by DFT. The complexes have square planar complexes geometry with slight distortion in both bond length and bond angle. The theoretical parameters have shown an excellent agreement with the experimental results and hence proved the reliability of the employed level of theory. The

resulting complexes exhibit quite good catalytic activity in comparison to those reported in the literature. The complex **1** exhibited excellent catalytic activity with the substrate containing bromo/iodo substituent. However, when the bromo substituent is in combination with aldehydes in the substrate, it exhibits higher catalytic activity in comparison to the combination of bromo and methoxy group. It was also observed from the DFT that the proposed intermediate is the π -complex which exhibit higher energy than σ -intermediate and it is situated at the top of the energy profile. Hence, it can be concluded that this catalytic system tolerates various functional group on the phenyl ring and could be further exploited for the design of promising catalytic material.

SUPPLEMENTARY MATERIAL

Physical, analytical and spectral data for the synthesized compounds are available electronically from <http://www.shd.org.rs/JSCS/>, or from the corresponding author on request.

Acknowledgements. The authors are grateful to the Principal, Government Science College, Jabalpur and Head, Chemistry Department, for providing necessary laboratory facilities. We sincerely thanks SAIF, CDRI, Lucknow, for recording ESI-MS, ^1H -NMR, ^{13}C -NMR and IISERBhopal for recording TGA. One of us (SSB) is also grateful to the UGC-New Delhi, for financial support through RGNF (Award letter no. F1-17.1/2017-18/RGNF-2017-18-SC-MAD 43228/(SAII/Website).

ИЗВОД

КАТАЛИТИЧКА ИСПИТИВАЊА Pd(II) КОМПЛЕКСА ПОМОЋУ HECK–MIZOROKI РЕАКЦИЈЕ: СИНТЕЗА, КАРАКТЕРИЗАЦИЈА И ТЕОРИЈА ФУНКЦИОНАЛА ГУСТИНЕ

SATYENDRA N. SHUKLA¹, PRATIKSHA GAUR¹, SANJAY S. BAGRI¹, RIPUL MEHROTRA²
И BHASKAR CHAURASIA¹

¹*Coordination Chemistry Research Lab, Department of Chemistry, Government Science College, Jabalpur (M.P.) 482001, India* и ²*Instituto de Quimica Rosario Area Inorganica Facultad de Cs. Bioquimicas y Farmaceuticas Universidad Nacional de Rosario Suipacha 531 S2002LRK Rosario, Argentina*

У реакцијама Шифових база као лиганада са паладијум(II)-хлоридом и имидазолом добијена су три комплекса опште формуле $[\text{Pd}(\text{II})(\text{L})(\text{imidz})_2]\text{Cl}$; L је 2-((E)-(p-алилимино)метил)-6-метоксиfenол (комплекс **1**), 2-метокси-6-((E)-(фенилимин)метил)фенол (комплекс **2**) и 2-((E)-(4-хлорофенилимино)метил)-6-метоксиfenол (комплекс **3**). Комплекси су охарактерисани на бази резултата елементалне микроанализе, моларне проводљивости, електронске спектроскопије, ESI-MS, FT-IR, TGA, ^1H -NMR и ^{13}C -NMR спектара. Молекулска структура и различити квантнохемијски параметри су одређени помоћу B3LYP базисног сета теорије функционала густине са стандардним 6-311+G(d,2p) нивоом. Каталитичка способност комплекса **1–3** испитивана је на основу Heck–Mizoroki реакције, при чему је нађено да се њихова катализичка способност мења у низу **1>2>3**.

(Примљено 2. септембра, ревидирано 18 новембра, прихваћено 20. новембра 2020)

REFERENCES

1. K. C. Nicolaou, P. G. Bulger, D. Sarlah, *Angew. Chem. Int. Ed.* **44** (2005) 4442 (<https://doi.org/10.1002/anie.200500368>)

2. C. Jia, T. Kitamura, Y. Fujiwara, *Acc. Chem. Res.* **34** (2001) 633 (<https://dx.doi.org/10.1021/ar000209h>)
3. A. Balanta, C. Godard, C. Claver, *Chem. Soc. Rev.* **40** (2011) 4973 (<https://dx.doi.org/10.1039/c1cs15195a>)
4. A. R. Hajipour, F. Rafiee, *J. Organomet. Chem.* **696** (2011) 2669 (<https://dx.doi.org/10.1016/j.jorganchem.2011.03.023>)
5. A. Dewan, U. Bora, G. Borah, *Tet. Lett.* **55** (2014) 1689 (<https://dx.doi.org/10.1016/j.tetlet.2014.01.041>)
6. F. Bakkali, S. Averbeck, D. Averbeck, M. Idaomar, *Food Chem. Toxicol.* **46** (2008) 446 (<https://dx.doi.org/10.1016/j.fct.2007.09.106>)
7. M. Esmaeilpour, J. Javidi, *J. Chin. Chem. Soc.* **62** (2015) 614 (<http://dx.doi.org/10.1002/jccs.201500013>)
8. R. F. Heck, *J. Am. Chem. Soc.* **90** (1968) 5518 (<https://doi.org/10.1021/ja01022a034>)
9. J. P. Genet, M. Savignac, *J. Organomet. Chem.* **576** (1999) 305 (<https://doi.org/10.1021/ja01022a034>)
10. M. Sankarganesh, N. Revathi, J. D. Raja, K. Sakthikumar, G. G. V. Kumar, J. Rajesh, M. Rajalakshmi, L. Mitu, *J. Serb. Chem. Soc.* **84** (2019) 291 (<https://dx.doi.org/10.2298/JSC180609080>)
11. H. O. Oloyede, J. A. O. Woods, H. Gorls, W. Plass, A. O. Eseola, *J. Mol. Struct.* **1199** (2020) 1 (<https://dx.doi.org/10.1016/j.molstruc.2019.127030>)
12. H. A. Doung, M. Cross, *J. Org. Lett.* **6** (2004) 4679 (<https://dx.doi.org/10.1021/o1048211m>)
13. P. J. Knowles, A. Whiting, *Org. Biomol. Chem.* **5** (2007) 31 (<https://dx.doi.org/10.1039/b611547k>)
14. C. S. Letizia, J. Cocchiara, J. Lalko, A. M. Api, *Food Chem. Toxicol.* **41** (2003) 943 ([https://dx.doi.org/10.1016/S0278-6915\(03\)00015-2](https://dx.doi.org/10.1016/S0278-6915(03)00015-2))
15. G. H. Jeffery, J. Bassett, J. Mendham, R. C. Denney, *Vogel's Textbook of Quantitative Inorganic Analysis*, 5th ed., John Wiley & Sons, Inc. New York, 1989
16. Y. Y. Yu, H. D. Xian, J. F. Liu, G. L. Zhao, *Molecules* **14** (2009) 1747 (<https://dx.doi.org/10.3390/molecules14051747>)
17. M. Amirnasar, A. H. Mahmoudkhani, A. Gorji, S. Dehghanpour, H. R. Bijanzadeh, *Polyhedron* **21** (2002) 2733 ([https://dx.doi.org/10.1016/S0277-5387\(02\)01277-9](https://dx.doi.org/10.1016/S0277-5387(02)01277-9))
18. N. Raman, Y. P. Raja, A. Kulandaishamy, *Proc. Indian Acad. Sci. (Chem. Sci.)* **113** (2001) 183
19. G. Y. Yeap, S. T. Ha, S. N. Ishizawa, K. L. Boey, W. A. K. Mahmood, *J. Mol. Struct.* **658** (2003) 87 ([https://dx.doi.org/10.1016/S0022-2860\(03\)00453-8](https://dx.doi.org/10.1016/S0022-2860(03)00453-8))
20. Gaussian Inc., Wallingford, CT, 2009
21. M. Dehestani, L. Zeidabadinejad, *J. Serb. Chem. Soc.* **80** (2015) 1008 (<https://dx.doi.org/10.2298/JSC150224027Z>)
22. D. A. Vicic, G. D. Jones, *Experimental Methods and Techniques: Basic Techniques*, Elsevier Ltd., University of Arkansas, Fayetteville, AR, 2007
23. W. J. Geary, *J. Coord. Chem. Rev.* **7** (1971) 81 ([https://dx.doi.org/10.1016/S0010-8545\(00\)80009-0](https://dx.doi.org/10.1016/S0010-8545(00)80009-0))
24. E. G. Bakirdere, M. F. Fellah, E. Canpolat, M. Kaya, S. Gur, *J. Serb. Chem. Soc.* **81** (2016) 520 (<https://doi.org/10.2298/JSC151030008B>)
25. M. Shabbir, Z. Akhter, I. Ahmad, S. Ahmed, M. Shafiq, B. Mirza, V. McKee, K. S. Munawar, A. R. Ashraf, *J. Mol. Struct.* **1118** (2016) 250 (<https://dx.doi.org/10.1016/j.molstruc.2016.04.003>)

26. A. A. Soliman, I. O. Alajrawy, A. F. Attabi, M. R. Shaaban, W. Linert, *Spectrochim. Acta, A* **152** (2016) 358 (<https://dx.doi.org/10.1016/j.saa.2015.07.076>)
27. Z. Leka, S. Grujic, Z. Tesic, S. Lukic, S. Skuban, S. Trifunovic, *J. Serb. Chem. Soc.* **69** (2004) 137 (<https://doi.org/10.2298/JSC0402137L>)
28. C. V. Barra, F. V. Rocha, A. V. G. Netto, R. C. G. Frem, A. E. Mauro, I. Z. Carlos, S. R. Ananias, M. B. Quilles, *J. Therm. Anal. Calorim.* **106** (2011) 489 (<https://dx.doi.org/10.1007/s10973-011-1393-0>)
29. S. A. Al-Jibori, M. M. Barbooti, M. H. S. Al-Jibori, B. K. Aziz, *J. Mater. Environ. Sci.* **8** (2017) 1365
30. V. G. Netto, A. M. Santana, A. E. Mauro, Regina C. G. Frem, *J. Therm. Anal. Calorim* **79** (2005) 339 (<https://doi.org/10.1007/s10973-005-0061-7>)
31. N. Yildirim, N. Demir, G. Alpaslan, B. Boyacioglu, M. Yildiz, H. Unver, *J. Serb. Chem. Soc.* **83** (2018) 707 (<https://dx.doi.org/10.2298/JSC171001009Y>)
32. T. A. Mohamed, I. A. Shaaban, R. S. Farag, W. M. Zoghaib, M. S. Afifi, *Spectrochim. Acta, A* **135** (2015) 417 (<https://dx.doi.org/10.1016/j.saa.2014.07.018>)
33. J. M. Collinson, Wilton-Ely, *J. Cat. Commun.* **87** (2016) 78 (<https://dx.doi.org/10.1016/j.catcom.2016.09.006>)
34. S. Layek, Anuradha. B. Agrahari, D. D. Pathak, *J. Organomet. Chem.* **846** (2017) 105 (<https://dx.doi.org/10.1016/j.jorgchem.2017.05.049>)
35. R. N. Prabhu, R. Ramesh, *Tetrahedron Lett.* **53** (2012) 5961 (<https://dx.doi.org/10.1016/j.tetlet.2012.08.120>)
36. C. S. Consorti, G. Ebeling, F. R. Flores, F. Rominger, *J. Adv. Synth. Catal.* **346** (2004) 617 (<https://dx.doi.org/10.1002/adsc.200303228>).